HYDROLOGICAL PROCESSES
Hydrol. Process. **23**, 597–611 (2009)
Published online 15 December 2008 in Wiley InterScience
(www.interscience.wiley.com) DOI: 10.1002/hyp.7188

Ensemble flood forecasting with stochastic radar image extrapolation and a distributed hydrologic model

Sunmin Kim,[1]* Yasuto Tachikawa,[2] Takahiro Sayama[1] and Kaoru Takara[1]

[1] *Disaster Prevention Research Institute, Kyoto University, Gokasho, Uji, Kyoto 611-0011, Japan*
[2] *Graduate School of Urban and Environmental Engineering, Kyoto University, C1, Nishikyo-ku, Kyoto 615-8540, Japan*

Abstract:

A new attempt on ensemble flood forecasting is introduced by use of a radar image extrapolation along with a stochastic error field simulation, and a distributed hydrologic model. In contrast to the conventional ensemble simulation that uses initial condition control to obtain a statistical outcome, stochastic prediction error fields were externally generated to offer probable variations of deterministic predictions. Firstly, a radar extrapolation model provided deterministic rainfall prediction, and its prediction error structure was analysed by comparing the observed rainfall fields. Secondly, on the basis of the analysed error structure, spatially correlated error fields were simulated using a covariance matrix decomposition method on a real-time basis. The simulated error fields enabled not only the production of probable rainfall field variations for ensemble simulation but also an improvement in prediction accuracy by offsetting the deterministic prediction error. Finally, the simulated error fields along with the deterministic fields were tested with a distributed hydrologic model to measure the validity of the ensemble runoff prediction. Copyright © 2008 John Wiley & Sons, Ltd.

KEY WORDS stochastic flood forecasting; ensemble; external error simulation; radar image extrapolation; distributed hydrologic model

Received 8 August 2006; Accepted 17 August 2007

INTRODUCTION

Nowcasting of precipitation is an essential prerequisite for real-time flood forecasting in operational hydrology. The term 'nowcasting' is used to emphasize the specificity and shortness ($0 \sim 3$ h) of rainfall forecast largely by radar image extrapolation, a method going back nearly 50 years (Smith and Austin, 2000; Fox and Wilson, 2005). Even though the benefits of short-term precipitation forecasts are well known, it is acknowledged as being among the most challenging areas in hydrology and meteorology (Collier and Krzysztofowicz, 2000).

Forecast techniques using radar observations are on the basis of tracking past movements of rain cells and extrapolating those movements. It does not usually allow for the growth and decay of the rainfall intensities or nonlinear motion of the rainfall band. The main disadvantage of this technique is that because of its simplicity, the forecast accuracy decreases rapidly within an hour (Bellon and Austin, 1984; Wilson *et al*., 1998). In a study of the improvement of forecast accuracy, elaborate nonlinear extrapolation schemes only give negligible improvement or even worse results than linear extrapolation (Smith and Austin, 2000).

Many hydrologists and meteorologists have conducted vast research efforts over several decades allowing for the introduction of many new schemes. These new schemes include mathematical and stochastic models integrated with a meteorological component (e.g. Georgakakos and Bras, 1984; Nakakita *et al*., 1996) and hybrid models, which are a combination of numerical weather prediction (NWP) and image extrapolation models (e.g. Golding, 2000; Ganguly and Bras, 2003). In addition, there have been complex statistical approaches such as using fractal generation algorithms (Lovejoy and Schertzer, 1986) and artificial neural networks (Grecu and Krajewski, 2000). However, even though there have been vast research efforts, it has still proven hard to find a notable improvement of forecast accuracy.

Extrapolation techniques are still in the mainstream for nowcasting, as many studies are taking place in order to develop more accurate extrapolation models (e.g. Kawamura *et al*., 1997; Georgakakos, 2000; Grecu and Krajewski, 2000). Even though there are many NWP models, these models still have insufficient spatial and temporal resolution to represent the detailed distribution of precipitation, and furthermore they require sophisticated data, which in many cases are unavailable (Golding, 2000). For this reason, radar image extrapolation is still a very powerful nowcasting tool in many practical flood forecasting situations.

For any natural phenomenon scientists try to forecast, one should bear in mind that there will always be an initial error in the model at the beginning of simulation and there will always be additional errors during a simulation because of the imperfection of the model's structure. To estimate the effect of the errors on the forecasting, it is necessary to supplement the deterministic forecasts

* Correspondence to: Sunmin Kim, Disaster Prevention Research Institute, Kyoto University, Gokasho, Uji, Kyoto 611-0011, Japan.
E-mail: sunmin@flood.dpri.kyoto-u.ac.jp

with detailed information regarding forecast reliability. For this reason, the stochastic concept has been included in forecasting, and ensemble simulation has been used as an effective tool for incorporating stochastic concepts into computer simulation. The ensemble forecast of hydrographs is also a recent trend away from the conventional simple deterministic forecasts of hydrographs and towards probabilistic forecasts, which include prediction uncertainty.

In atmospheric modelling, small perturbations of the initial condition and/or boundary condition in the beginning of a model simulation have been used as a trigger for ensemble forecasting (e.g. Du and Mullen, 1997). Most of the ensemble simulations in the early stages have been concerned only with the internal growth of initial error and therefore, have been criticized for underestimating the total uncertainty as not all sources of uncertainty are accounted for in the ensemble generator (Leith, 1974; Krzysztofowicz, 2001). In considering the additional growth of prediction error rising from an imperfect model structure, external error consideration should be contemplated.

As a step towards addressing the improvement of forecast accuracy and stochastic forecasting with consideration of external error, this study introduces a new attempt at ensemble rainfall forecasting using a radar image extrapolation and a stochastic error field simulation. The simulated prediction error not only gives probable rainfall field variations for the ensemble simulation but also improves the accuracy of the deterministic prediction by correcting the possible prediction error. Then, stochastic prediction fields are given to a distributed hydrologic model to achieve ensemble runoff predictions.

The organization of this paper is as follows. First, an illustration is given of a method of deterministic prediction of rainfall using a radar image extrapolation as well as the analysis of its prediction error pattern. Second, the main algorithm for the generation of stochastic error field is given, and ensemble forecasting of rainfall is performed on the basis of the proposed algorithm. Then, the rest of this paper evaluates the ensemble forecast results for both precipitation and runoff discharge. Finally, the main conclusions are outlined.

NOWCASTING WITH RADAR IMAGE EXTRAPOLATION AND ITS ERROR STRUCTURE

Introduction of the translation model

The translation model by Shiiba *et al*. (1984) is used in this study for deterministic predictions of short-term radar rainfall. In this model, the horizontal rainfall intensity distribution, $z(x, y, t)$ with the spatial coordinate (x, y) at time t is defined as

$$\frac{\partial z}{\partial t} + u\frac{\partial z}{\partial x} + v\frac{\partial z}{\partial y} = w \qquad (1)$$

$$u = \frac{dx}{dt},\ v = \frac{dy}{dt},\ w = \frac{dz}{dt}$$

where, u and v are advection velocity along x and y, respectively, and w is rainfall growth-decay rate with time. As with other similar discrete equations for the rainfall intensity distribution, characteristics of the translation model are defined by the vectors u, v and w, which are specified on each grid as follows:

$$u(x, y) = c_1x + c_2y + c_3$$
$$v(x, y) = c_4x + c_5y + c_6$$
$$w(x, y) = c_7x + c_8y + c_9 \qquad (2)$$

As such, the advection velocities can express the patterns of the non-uniform movement of rainfall, such as rotation and sheer strain (Takasao *et al*., 1994). In order to optimize the parameters $c_1 \sim c_9$ using observed radar rainfall data, Equation (2) is approximated by the central difference scheme on the rectangular horizontal area with $\Delta x \times \Delta y$ grid size and Δt time resolution.

$$x_i = (i - \frac{1}{2})\Delta x, \qquad i = 1, \cdots, M$$
$$y_i = (j - \frac{1}{2})\Delta y, \qquad j = 1, \cdots, N$$
$$t_k = k\Delta t, \qquad k = -(K-1), \cdots, 0 \qquad (3)$$

Here, M and N are the number of grids along the x and y-axis, respectively, and K is the number of rainfall patterns used for the optimization. The parameters $c_1 \sim c_9$ are sequentially optimized using the square root information filter in a manner of minimizing

$$J_c = \sum_{k=-K}^{-1}\sum_{i=2}^{M-1}\sum_{j=2}^{N-1} v_{ijk}^2 \qquad (4)$$

where,

$$v_{ijk} = \left[\frac{\Delta z}{\Delta t}\right]_{ijk} + (c_1x_i + c_2y_j + c_3)\left[\frac{\Delta z}{\Delta x}\right]_{ijk} + (c_4x_i + c_5y_j + c_6)\left[\frac{\Delta z}{\Delta y}\right]_{ijk} - (c_7x_i + c_8y_j + c_9)$$

The translation model provides expected rainfall movements under an assumption that the vectors u and v are time invariant for the next several hours and that there is no growth-decay of rainfall intensities during that time. In this study, three consecutive observed rainfall fields, which have a resolution of 3 km and 5 min, are used to determine u and v. When forecasting rainfall fields, the u and v are assumed spatially uniform and updated every 5 min. Most heavy rainfall events in Japan, which occur during the rainy and typhoon season, have a frontal rain band over several hundred kilometers, and therefore the movement of the rainfall band can be considered to be spatially uniform within a single radar range that has a 120-km radius.

Deterministic prediction of precipitation and its error structure

Radar data used for testing the translation model are observed at the Miyama radar station located in

DOI: 10.1002/hyp

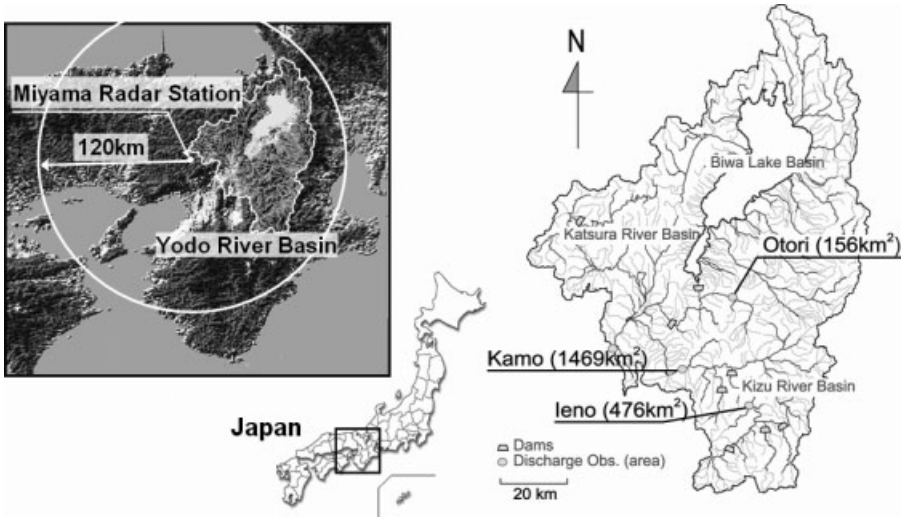

Figure 1. Miyama radar station (120-km radius circle) and Yodo-River basin, which includes Ootori, Ieno, and Kamo stations for ensemble discharge prediction analysis

the central part of Kinki district, Japan (Figure 1). The observation field of the radar includes all spaces within a radius of 120 km and a height of 15 km (for details on the radar station refer to Nakakita *et al*., 1990). It takes 5 min to scan over the entire observation field and therefore rainfall reflectivity data are produced every 5 min. The reflectivity data are converted to rainfall intensity of a 3-km spatial resolution by the Z-R relationship, $Z = 200R^{1.6}$ according to Marshall and Palmer (1948). During the conversion, basic correction for ground clutter and shadow effects is carried out. The converted rainfall intensity, which is called observed rainfall field in this study, was used as a reference value for the accuracy improvements of prediction fields.

Two representative rainfall events have been selected for this study. Those events are of a typical frontal rain band type, which occurred during the rainy season (June and July) and the typhoon season (August and September) in Japan. Details of the selected events are illustrated in Table I. One event that took place in August of 1992 had severe rainfall intensity with rapid changes in velocity, while the event of June 1993 had a rather steady and slowly moving rainfall band.

Figure 2 shows the characteristics of forecasted rainfall by the translation model for 60, 120, and 180-min lead-times. First of all, Figure 2a shows the spatially averaged rainfall intensities of observation and each prediction for the August 1992 event. In order to prevent outside influence from the size and shape of rainfall bands, the intensity calculation includes every grid within the radar observation domain. Note that there are overall delays of rainfall intensities, as prediction time elongates.

Table I. Radar data and its characteristics

Title	Duration	Type
August 1992 event	92/8/18 ~ 19	Typhoon season (frontal)
June 1993 event	93/6/30 ~ 31	Rainy season (frontal)

Because the translation model used here only represents the movement of the rainfall bands without their growth or decay, the model assumes the same amount of current rainfall intensities lasts until the prediction target time.

In Figure 2b, correlation coefficients (CCs) of the observation and predictions are shown. The majority of the time, CC values are under 0·5, which is a rather low value. As it can be expected, the coefficients with short lead-time have higher values compared to longer lead-time predictions.

Another method used to measure prediction accuracy is the critical success index (CSI), which is widely adopted in forecast verification in the form of

$$CSI(\%) = \frac{X}{X + Y + Z} \times 100 \tag{5}$$

where, X is the number of correctly forecasted rainfall cells (i.e. rainfall is observed and also predicted in the grid), Y is the number of misses (i.e. rainfall is observed, but not predicted), and Z is the number of false alarms (i.e. rainfall is predicted, but not observed). A threshold rain-rate for the CC and CSI is over 0·0 mm/h in this study.

The CSI show rather high values in most prediction times even for the 180-min prediction (Figure 2c). In the figure, the index clearly shows that shorter lead-time predictions have higher prediction accuracy compared to longer lead-time. The index appeared to have a positive relationship to the covering area of rainfall bands. This is rather a reasonable phenomenon since the index can be simply regarded as an overlap ratio of the prediction rainfall band to the observed band.

Tachikawa *et al*. (2003) statistically analysed the characteristics of prediction error and relative prediction error and defined them as shown in Equations (6) and (7).

$$E_{a,i} = R_{o,i} - R_{p,i} \tag{6}$$

$$E_{r,i} = (R_{o,i} - R_{p,i})/R_{p,i} \tag{7}$$

DOI: 10.1002/hyp

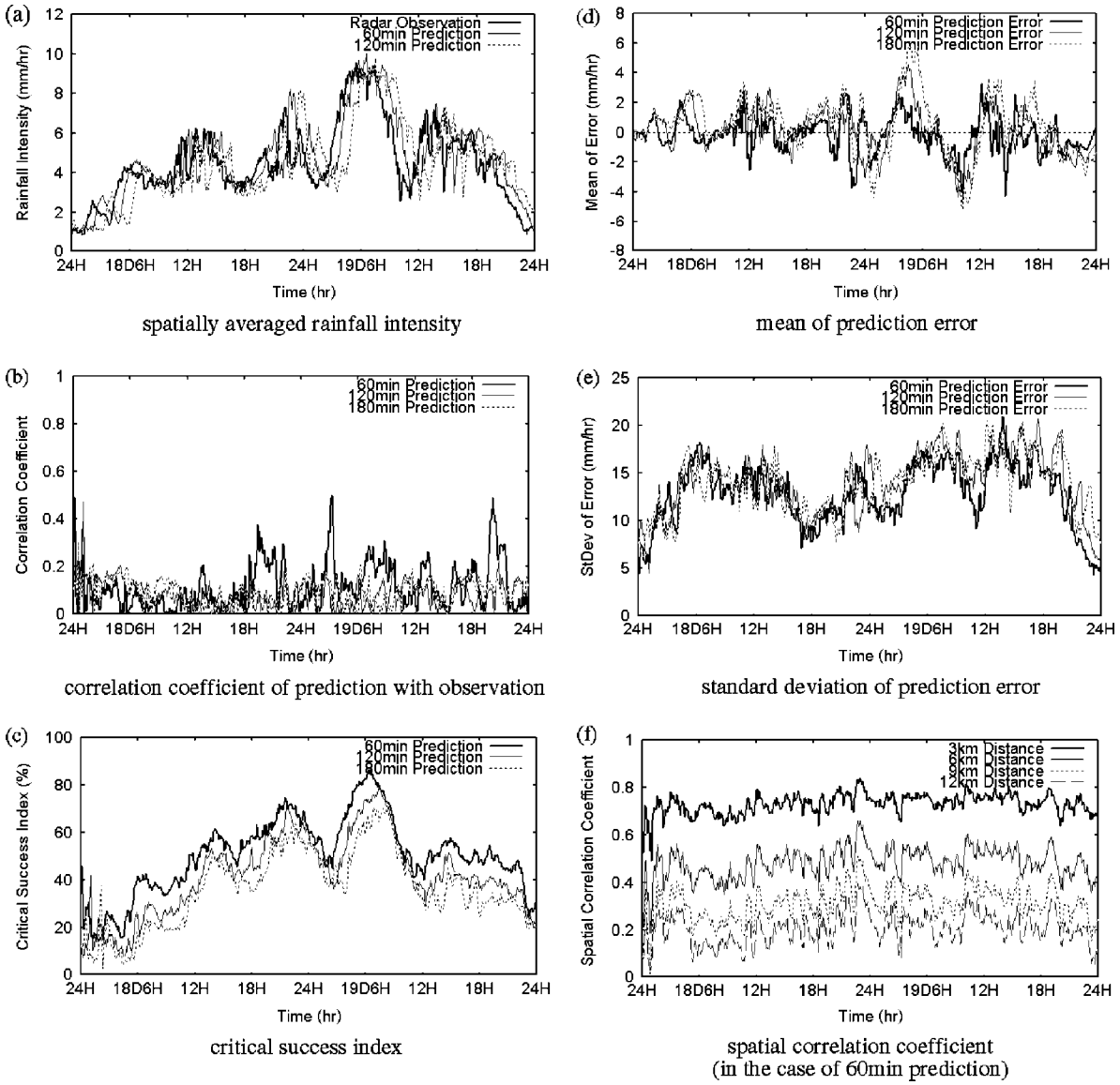

Figure 2. Deterministic prediction results from the translation model. Spatially averaged rainfall intensities (a), performance index [correlation coefficient (b) and critical success index (c)], and the error characteristics [mean (d) and standard deviation (e) of the error and spatial correlation coefficient (f)] in the case of August 1992 event

The prediction error $E_{a,i}$ on a certain grid i is calculated from the difference between predicted rainfall $R_{p,i}$ and observed rainfall $R_{o,i}$ on the grid, while the relative prediction error $E_{r,i}$ is the ratio of the prediction error to its predicted rainfall. Tachikawa *et al.* (2003) examined the temporally accumulated error values with variant spatial resolutions and found that the distributions of the prediction error and relative prediction error are respectively close to normal distribution and lognormal distribution.

This study concentrates on the prediction error $E_{a,i}$ and simulates the spatially correlated possible error for future prediction target times on a real-time basis. Basic statistics of the prediction error examined in this study include the mean and standard deviations as well as the probability distribution of the error, which indicates normal distribution allowing a slight variation in each event and prediction case. Figure 2d and e show basic statistics of 60, 120, and 180-min prediction error for the August 1993 event. The spatial correlation coefficients (SCCs)of $E_{a,i}$, which shows how much the errors are spatially correlated to each other, is calculated for every time step by grouping every pair of errors having the same distance on each error field. The SCC in Figure 2f shows high values for close distances and decreases as the distance increases, and the error from longer prediction times has higher SCC values than the error from shorter prediction times. In most prediction cases, the sccs decrease drastically at a distance of 10 km, as shown in Figure 2f with the 60-min prediction case.

For reviewing the spatial pattern of the prediction error, the errors on each grid are accumulated event by event. For example, if there is a certain spatial and/or temporal pattern in the prediction error, because of perpetual overestimation or underestimation on a certain area during a certain event, the accumulated error

DOI: 10.1002/hyp

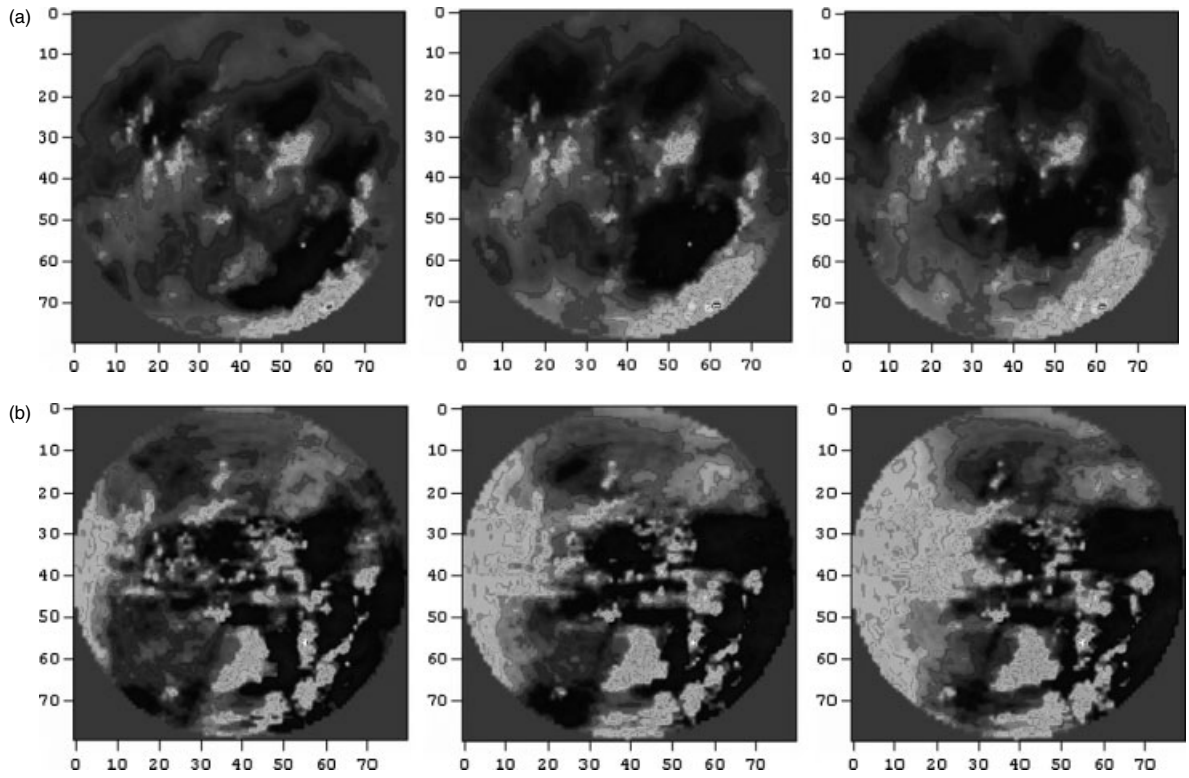

Figure 3. Accumulation of the prediction error during each event (unit: mm/h). There is a specific spatial pattern on each accumulation, and it presents localized overestimation or underestimation on a certain area

will present those patterns. Otherwise, if the error does not have any spatiotemporal pattern namely arbitrarily random errors, the accumulated prediction error on every grid would compensate each other.

As shown in Figure 3, there is a specific spatial pattern on each accumulation of prediction error. Note that although each individual event depicts similar spatial error patterns within itself, prediction error patterns are different from event to event. The error would have a complex relationship with topography as well as meteorological conditions of each event, and it is difficult to define the error beforehand. Thus, in the next section, a method to obtain a spatially variant error pattern on a real-time basis is proposed and it is used for stochastic prediction in this study.

STOCHASTIC FORECASTING OF PRECIPITATION WITH PREDICTION ERROR FIELD

Prediction error field simulation algorithm

The main purpose of the algorithm is to simulate possible error fields using the current prediction error structure including its spatial correlation. This is conducted under the assumption that a temporal persistence of the error characteristics continues from the current time to the prediction target time. The proposed scheme uses a certain time length of previous prediction error data to simulate future prediction errors as shown in Figure 4.

In Figure 4, the observed rainfall fields, the deterministic prediction fields, and the prediction error fields are sequentially illustrated until the current time t. Although distinct prediction fields having different lead-time can exist on each time step, for the sake of simplicity only one prediction lead-time ΔT is considered in the figure. Again, every prediction field at each time step is the prediction result that is obtained at ΔT before that time. At the current time t, the translation model carries out prediction for the time $t + \Delta T$; then the probable prediction error of the prediction is simulated in accordance with the current error characteristics.

The current characteristics of the prediction error can be presented by basic statistics under an assumption that the time series of the error on each grid follows normal probability distribution. Here, the basic statistics stand for the mean and standard deviation values of the most recent errors in certain time length on each grid. On the basis of this procedure, the 'error statistic field' can incorporate spatial and temporal characteristics of the current errors and is updated on a real-time basis.

If the spatiotemporal characteristics of the prediction error lasts for several hours, and the statistical characteristics of the error on the prediction target time $t + \Delta T$ are similar to the characteristics of the current error, the possible error fields at $t + \Delta T$ can be simulated by using the error statistic field. This assumption regarding the temporal persistency of the error characteristics is evaluated in the next section.

Figure 5 explains the procedure for the simulation of the possible prediction error. The 'error statistic field' and the mean and standard deviation fields of the current prediction error (Figure 5b and d), convert the 'unit random error field' (Figure 5c) to the target error field

DOI: 10.1002/hyp

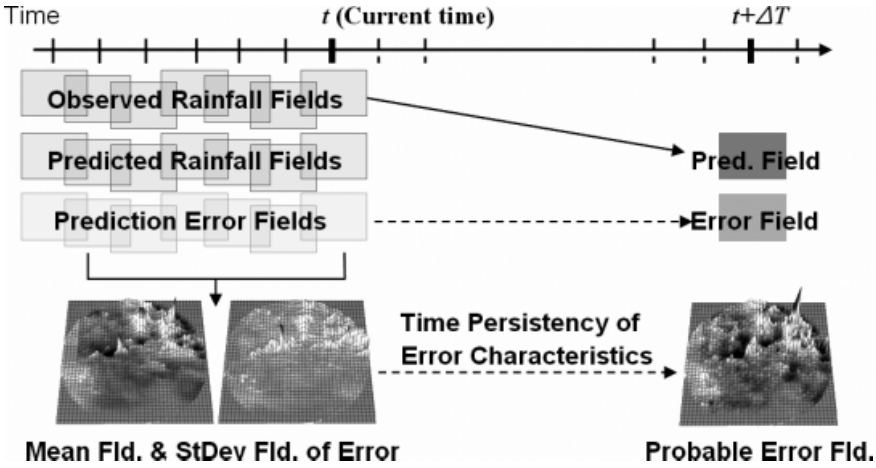

Figure 4. Schematic drawing of the algorithm for a stochastic error field simulation. At the current time t, the translation model carries out prediction for the time $t + \Delta T$; then the probable prediction error of the prediction is simulated in accordance with the current error characteristics

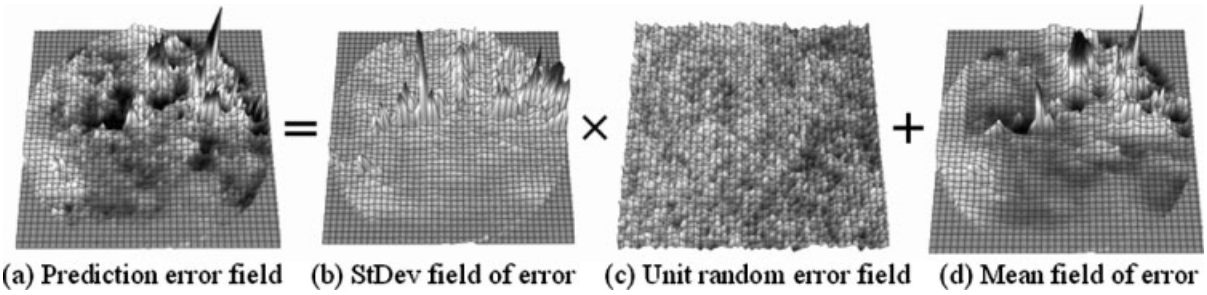

Figure 5. Simulation procedure of prediction error field using error statistic field and unit random error field. The 'error statistic field', the mean, and standard deviation field of the current prediction error converts the 'unit random error field' comprised of spatially correlated random numbers of $N(0,1)$ to the prediction error field

(Figure 5a). The unit random error field is a set of random values, which are spatially correlated to each other and are assumed to follow the normal distribution of $\mathbf{N}(0,1)$. Through numerous generations of the unit random error field, it becomes possible to acquire various error fields for the prediction target time. Finally, the deterministic prediction field by the translation model is extended to many prospective prediction fields by combining them with the simulated error fields. Details of this procedure are discussed in the following section.

Time persistency of the error characteristics

To verify the temporal persistence of the characteristics of prediction error, the modified critical success index (MCSI) in Equation (8) is proposed. The MCSI uses the same form of CSI, shown in Equation (5), with the exception of range concept. As noted in the previous section, the error statistic field gives a specific probabilistic range on each grid by the mean μ and the standard deviation σ of the error on its own grid. If the analysed prediction error of the target time on a certain grid is within the range $\mu - \sigma$ and $\mu + \sigma$ on the grid, it is counted as a correct value, X, and if the error is out of the range, it is counted as an incorrect value, Y.

$$MCSI(\%) = \frac{X}{X+Y} \times 100 \tag{8}$$

Since the probability within the unit variance in a standard normal distribution is 0·6826, the expected MCSI value in this analysis is around 68%. Evaluations were conducted with three different sets of error statistic fields generated from different time lengths of error data: 10, 30, and 60 min. Figure 6 shows the MCSI values for the 60-min lead-time predictions with three different error statistic fields. In the results from the August 1992 event, the MCSI using the one of 30-min time length starts with high values around 80%, and lowers as the rainfall intensity becomes stronger. When it is considered that most MCSI values are over 60%, this result is highly encouraging for adopting the time persistence of the prediction error.

Compared to the MCSI using the 30-min time length of error statistic field, the 60-min time length one has larger values, whereas the 10-min time length one indicates lower values. When the error statistic fields of different time lengths were compared to each other, the mean field of error did not show significant differences. However, the longer the time length of an error statistic field is, the larger the produced standard deviation value is; therefore the value X can have bigger values in MCSI.

In this study, the 30-min time length of the error statistic field is used for the error field simulation in the next section. Tables II and III show the time averaged MCSI values for different lead-times (60, 120, and 180-min prediction) from both events.

DOI: 10.1002/hyp

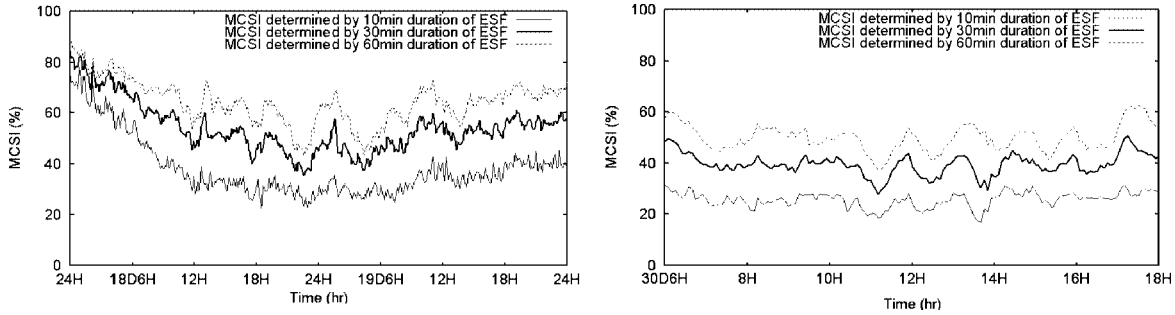

Figure 6. MCSI determined by different durations of error statistic field (ESF), which shows highly encouraging results (over 68%) for adopting the time persistence of the prediction error [from the 60-min prediction of the August 1992 event (left) and the June 1993 event (right)]

Table II. Averaged *MCSI* values from variant prediction lead-times (August 1992 event, Unit: %)

Lead-time	Time lengths to determine error statistics		
	10 min	30 min	60 min
60-min prediction	37·88	53·92	64·13
120-min prediction	35·43	50·52	60·48
180-min prediction	35·83	50·59	60·09

Table III. Averaged *MCSI* values from variant prediction lead-times (June 1993 event, Unit: %)

Lead-time	Time lengths to determine error statistics		
	10 min	30 min	60 min
60-min prediction	25·69	39·46	49·95
120-min prediction	21·75	32·90	42·66
180-min prediction	23·30	34·12	42·48

Spatially correlated random error field

The simulation of the unit random error field is on the basis of the decomposition of a matrix that includes spatial correlation characteristics of the prediction error in a covariance matrix form. The matrix is decomposed approximately into its square root matrix with the matrix factorization technique and the Chebyshev polynomials (Davis, 1987; Tachikawa and Shiiba, 2000). Multiplying the square root matrix by a random vector $\mathbf{N}(0,1)$ gives a non-conditional simulation of the unit random error field.

Davis (1987) proved a symmetric matrix $\mathbf{B}$ that satisfies $\mathbf{K} = \mathbf{BB}$ could be found when $\mathbf{K}$ is symmetric and positive-definite. The random vector $\mathbf{Y}$ (in this study, the spatially correlated unit random error) can be written as

$$\mathbf{Y} = \mathbf{Bw}$$

Where, $\mathbf{w}$ is the uncorrelated random vector $\mathbf{N}(0,1)$. The expected value of the matrix $\mathbf{YY}^{\mathrm{T}}$ (n × n) is given by

$$\mathrm{E}[\mathbf{YY}^{\mathrm{T}}] = \mathrm{E}[\mathbf{Bww}^{\mathrm{T}}\mathbf{B}^{\mathrm{T}}] = \mathbf{B}\mathrm{E}[\mathbf{ww}^{\mathrm{T}}]\mathbf{B}^{\mathrm{T}}$$

Because $\mathbf{w}$ is a vector of independent random numbers, $\mathrm{E}[\mathbf{ww}^{\mathrm{T}}] = \mathbf{I}$, and thus,

$$\mathrm{E}[\mathbf{YY}^{\mathrm{T}}] = \mathbf{BIB}^{\mathrm{T}} = \mathbf{K}$$

The SCCs, which are obtained from the prediction error E_a, make up the covariance matrix $\mathbf{K}$.

$$K = \begin{bmatrix} scc_0 & scc_1 & scc_2 & \cdots & scc_n \\ scc_1 & scc_0 & scc_1 & \cdots & scc_{n-1} \\ scc_2 & scc_1 & scc_0 & \cdots & scc_{n-2} \\ \vdots & \vdots & \vdots & \ddots & \vdots \\ scc_n & scc_{n-1} & scc_{n-2} & \cdots & scc_0 \end{bmatrix} \quad (9)$$

Equation (9) shows the basic form of the matrix $\mathbf{K}$. Under an assumption of ergodicity on scc, the scc_j is prepared using two error groups, which are j grids separate from each other within one error field. Since the variation of each scc_i does not vary with time (Figure 2f), time averaged scc_i from the 30-min time length of error statistic fields is used for the matrix $\mathbf{K}$ in this study.

The matrix $\mathbf{K}$ is decomposed into a symmetric matrix $\mathbf{B}$ approximately by the Chebyshev polynomials. Vector $\mathbf{Y}$ (or unit random error field), which is a non-conditional simulation of spatially correlated random vectors, can be generated continuously by multiplying the matrix $\mathbf{B}$ by an uncorrelated random vector $\mathbf{w}$.

The error statistic field converts the unit random error field to the error fields as shown in Equation (10):

$$\begin{bmatrix} E_{\mathrm{s},1} \\ E_{\mathrm{s},2} \\ E_{\mathrm{s},3} \\ \vdots \\ E_{\mathrm{s},n} \end{bmatrix} = \begin{bmatrix} sd_0 & 0 & 0 & \cdots & 0 \\ 0 & sd_1 & 0 & \cdots & 0 \\ 0 & 0 & sd_2 & \cdots & 0 \\ \vdots & \vdots & \vdots & \ddots & \vdots \\ 0 & 0 & 0 & \cdots & sd_n \end{bmatrix} \begin{bmatrix} y_1 \\ y_2 \\ y_3 \\ \vdots \\ y_n \end{bmatrix} + \begin{bmatrix} m_1 \\ m_2 \\ m_3 \\ \vdots \\ m_n \end{bmatrix} \quad (10)$$

Here, the m_i and sd_i are the mean and standard deviations of the current prediction error on grid i. The y_i is the unit random error of the vector $\mathbf{Y}$, and the $E_{\mathrm{s},i}$ is the simulated error for the prediction target time. Equation (10) is a linear equation, thus the spatial correlation structure of $\mathbf{Y}$, which is obtained from E_a, is maintained in E_s. The form of Equation (10) is identical to Figure 5, and the total grid number of the Miyama radar image is 80×80, thus the n in Equation (10) is

DOI: 10.1002/hyp

6400. Fifty sets of error fields at each time increment were generated for an ensemble simulation.

Generation of stochastic prediction fields

Deterministic predictions from the translation model are extended to many stochastic prediction fields by combining them with the simulated error fields as follows:

$$R_{s,i} = R_{p,i} + E_{s,i} \qquad (\approx R_{o,i} = R_{p,i} + E_{a,i}) \tag{11}$$

where, $E_{s,i}$ is the simulated prediction error value on grid i, $R_{p,i}$ is the prediction from the translation model, and $R_{s,i}$ is the stochastic prediction. Because the simulated prediction error contains the error statistics of the prediction error ($E_{s,i} \approx E_{a,i}$), the stochastic prediction can be close to the observed rainfall on the prediction target time ($R_{s,i} \approx R_{o,i}$).

Because some values on the simulated error field yield negative values that can be larger than the predicted rainfall values at that point, negative values could occur on the stochastic prediction fields. These negative rainfall values are set to zero, and the same amount of negative values is subtracted from the positive rainfall values so as to keep the total rainfall amount as

$$\begin{aligned} R'_{s,i} &= R_{s,i}(1+r) \qquad (\text{if } R_{s,i} \geq 0{\cdot}0) \\ &= 0{\cdot}0 \qquad\quad (\text{if } R_{s,i} < 0{\cdot}0) \end{aligned} \tag{12}$$

$$\text{here, } r = \frac{\sum NegativeR}{\sum PositiveR}$$

Here, the value r stands for the ratio of the total negative rainfall amount on each stochastic prediction field to the total positive rainfall amount. The total amount of negative rainfall generally is 10–20% of the total positive rainfall amount; therefore, r varies from −0·1 to −0·2. In addition to tallying total rainfall amount, this procedure gives a smoothing effect on the stochastic prediction fields, so that it decreases abnormally high prediction values.

RESULTS AND EVALUATION OF THE STOCHASTIC PREDICTION FIELDS

Spatially averaged rainfall intensities are checked as shown in Figure 7a with the 60-min prediction of the August 1992 event. The intensities from the stochastic prediction fields make a certain range and show similar patterns of intensities in the deterministic prediction. If the bias correction mentioned in the previous section works properly, the stochastic prediction fields should have values that are more accurate. As shown in Figure 7b, the spatial mean of absolute error at each time step from the stochastic prediction have smaller values than the error from the deterministic prediction. The CCs from the stochastic prediction also show improved results in most prediction times (Figure 7c). In most prediction times, the coefficients from the stochastic prediction fields have higher values compared to the values from the deterministic prediction. Yet, the CSI values in Figure 7d do not show a vast difference between the stochastic prediction and the deterministic prediction. Because the error field simulation is on the basis of the most recent prediction results, theoretically, the simulated error field

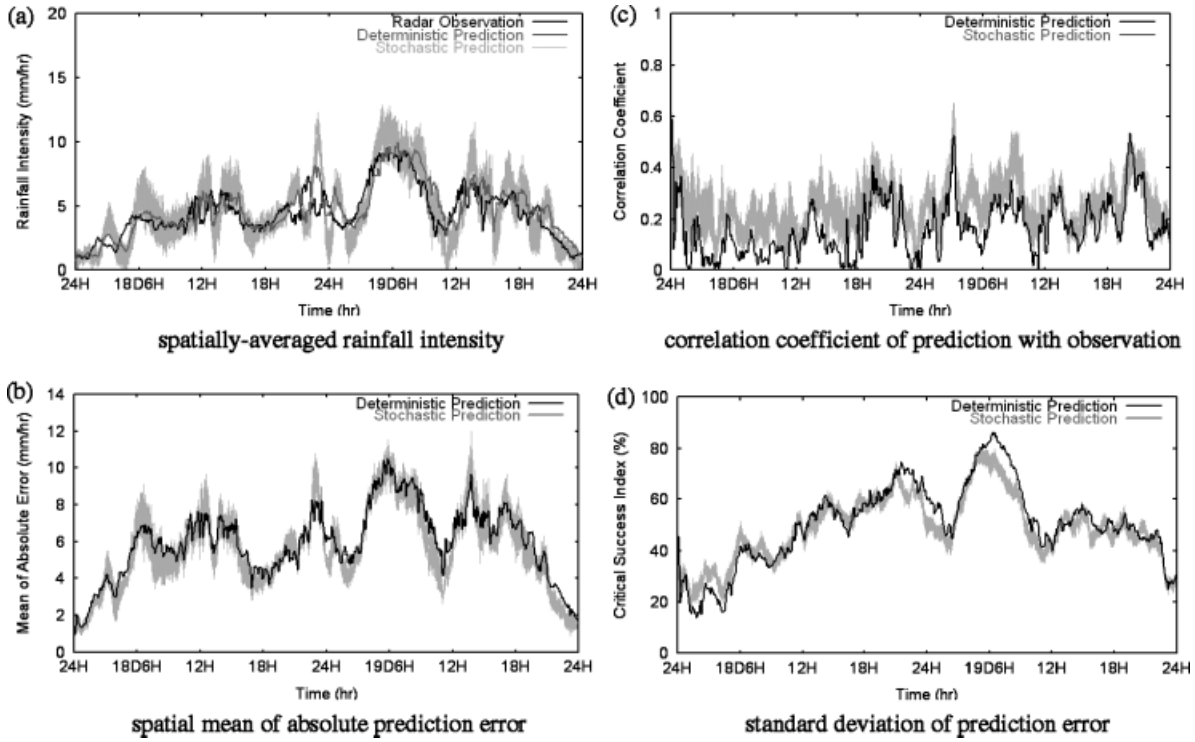

Figure 7. Verification of stochastic prediction of precipitation (August 1992 event). The stochastic prediction fields show improved accuracy [smaller spatial mean of absolute prediction error (b) and higher correlation coefficient (c)] with its reliability range (d) critical success index

DOI: 10.1002/hyp

contains the same area as the prediction fields, and therefore it does not significantly alter the CSI values. More detailed verification will be discussed in the following sections.

Forecast verification

For an overall forecast verification, several performance indices were adopted, such as accumulated rainfall amounts (ACRAs), root mean square error (RMSE) and mean of absolute error (MAE). Firstly, ACRA is total amount of the observation and prediction (whether it is deterministic or stochastic) given as

$$ACRA = \sum_{t=1}^{n_t}\left(\frac{1}{n_s}\sum_{s=1}^{n_s} O_{t,s}\right) \quad or$$
$$= \sum_{t=1}^{n_t}\left(\frac{1}{n_s}\sum_{s=1}^{n_s} F_{t,s}\right) \tag{13}$$

where, n_s and n_t are the numbers of rainfall grids and time steps. $O_{t,s}$ and $F_{t,s}$ are observed and predicted values at time t on point s. Note that the observed values $O_{t,s}$ may be different from the ground gauge observation, since the radar observation used in this study is not adjusted to the ground gauge data. However, this radar observation $O_{t,s}$ is regarded as the reference rainfall value of the prediction. For the ensemble forecasting results, which has 50 sets of the stochastic prediction field, the mean and standard deviations of the ACRA were calculated, and the minimum as well as maximum of the ACRA values was also examined.

Secondly, the performance indices adopted to obtain a single overall score are RMSE and MAE as expressed in Equations (14) and (15).

$$RMSE = \frac{1}{n_t}\sum_{t=1}^{n_t}\left(\sqrt{\frac{1}{n_s}\sum_{s=1}^{n_s}(O_{t,s}-F_{t,s})^2}\right) \tag{14}$$

$$MAE = \frac{1}{n_t}\sum_{t=1}^{n_t}\left(\frac{1}{n_s}\sum_{s=1}^{n_s}|O_{t,s}-F_{t,s}|\right) \tag{15}$$

Lastly, time averaged CC and CSI were examined. These are simply the mean of the CC and CSI values' time series for a perspective comparison of variant prediction lead-time.

$$MCC = \frac{1}{n_t}\sum_{t=1}^{n_t} CC_t \tag{16}$$

$$MCSI = \frac{1}{n_t}\sum_{t=1}^{n_t} CSI_t \tag{17}$$

For an ensemble simulation result, which has fifty stochastic predictions, mean of RMSE, MAE, MCC and MCSI values are calculated and compared with the values from the deterministic prediction.

Verification results and discussion

Figure 8 and Table IV show the comparison of ACRA values of observation, deterministic and stochastic prediction from the variant prediction lead-time of the August 1992 event. Better results having closer ACRA value to the observed one are marked with bold character in Table IV. In the figure, ACRA value of the observation is presented with a solid line parallel with the x-axis, which represents the prediction lead-time. The ACRA values from the deterministic and stochastic prediction are expressed with points and error-bars.

The ACRA values from the deterministic prediction decrease as prediction lead-time get longer, showing some differences to the observed one. The reason of the decrease can be found in the simulation behaviour of the translation model. When the model performs a simulation, the optimized u and v vectors transfer the current rain bands, and therefore some rainfall area is located outside of the radar range at the prediction target time. In addition, because new rain band that comes in the radar range during the simulation is not counted in the prediction results, the deterministic prediction shows a trend of decreasing rainfall area as well as the ACRA values. However, the error field simulation of this study incorporates the information of the newly added rain bands, and as a result, the stochastic prediction shows relatively steady ACRA values regardless of the prediction lead-time.

The reliability range of the stochastic forecasting (whether the standard deviation, or the maximum and minimum values) clearly expresses the uncertainty of the forecasted values; the larger the prediction lead-time is extended, the wider the range becomes.

Figure 9 and Table V show the comparison of ACRA values from the June 1993 event. In the figure, ACRA values of the deterministic prediction show a larger discrepancy to the observation as the lead-time is longer. While the mean values of the stochastic prediction also show some discrepancy to the one from the radar observation, the range of the stochastic prediction successfully encompasses the observation values.

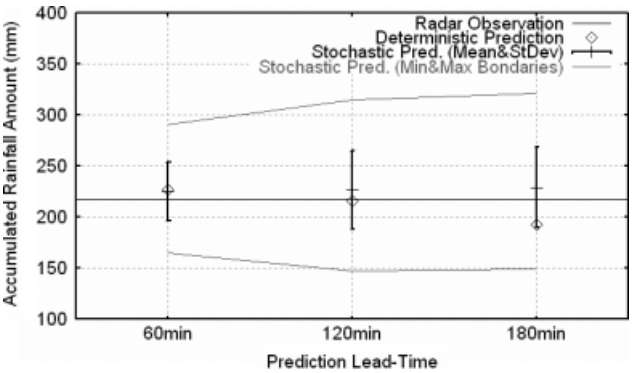

Figure 8. Accumulated rainfall amounts (ACRA) for August 1992 event (high rainfall intensity). The stochastic prediction shows relatively steady ACRA values regardless of the prediction lead-time, and the reliability range (the standard deviation, or the maximum and minimum values) clearly expresses the uncertainty of the forecasting

DOI: 10.1002/hyp

Table IV. Accumulated rainfall amount (ACRA) values (August 1992 event, Unit: *mm/h*)

Lead-time	Observation	Deterministic prediction	Stochastic prediction	
			Mean±StDev	Min∼Max
60-min prediction	217·38	226·64	**224·79** ± 28·51	165·09 ∼ 290·06
120-min prediction	217·38	**215·94**	226·29 ± 38·29	147·15 ∼ 314·78
180-min prediction	217·38	192·17	**228·97** ± 39·74	149·04 ∼ 321·40

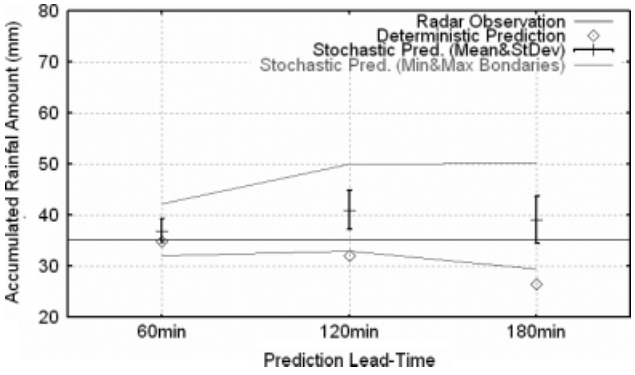

Figure 9. Accumulated rainfall amounts comparison for June 1993 event (low rainfall intensity). While the mean values of the stochastic prediction show some discrepancy to the radar observation, the ranges of the stochastic prediction encompass the observation values

Tables VI and VII show the RMSE and MAE from the variant forecast lead-times of the August 1992 event and June 1993 event. The values for the 'stochastic' in the table are averaged values from the 50 sets of stochastic prediction results. The August 1992 event clearly illustrates that the stochastic prediction gives much smaller error values than the deterministic prediction in all lead-times. Furthermore, both scoring values become larger for longer lead-times, which show higher uncertainty for longer lead-time predictions. On the other hand, the June 1993 event resulted in better values for the deterministic prediction than for the stochastic prediction. This may be because the June 1993 event has low rainfall intensities and therefore, the stochastic predictions are much more influenced by the negative rainfall handling during the stochastic prediction field simulation. However, undefined spatial and/or temporal characteristics in a certain rainfall pattern can be there during the June 1993 event and therefore, more detailed study with various event types is required in order to generalize the proposed stochastic prediction method.

The mean of correlation coefficient (MCC) and MCSI for the August 1992 event and June 1993 event are respectively presented in Tables VIII and IX. The values for the 'stochastic' in the table are averaged values from

Table V. Accumulated rainfall amount (ACRA) values (June 1993 event, Unit: *mm/h*)

	Observation	Deterministic prediction	Stochastic prediction	
			Mean±StDev	Min∼Max
60-min prediction	35·14	**34·81**	36·88 ± 2·30	31·97 ∼ 42·28
120-min prediction	35·14	**32·01**	40·98 ± 3·85	32·85 ∼ 49·97
180-min prediction	35·14	26·42	**39·06** ± 4·67	29·39 ∼ 50·06

Table VI. Root mean square error (RMSE) and mean of absolute error (MAE) (August 1992 event, Unit: *mm/h*)

Lead-time	RMSE		MAE	
	Deterministic	Stochastic	Deterministic	Stochastic
60-min prediction	12·97	**11·50**	5·96	**5·36**
120-min prediction	14·01	**12·17**	6·60	**5·86**
180-min prediction	14·06	**12·59**	6·58	**6·19**

Table VII. Root mean square error (RMSE) and mean absolute error (MAE) (June 1993 event, Unit: *mm/h*)

Lead-time	RMSE		MAE	
	Deterministic	Stochastic	Deterministic	Stochastic
60-min prediction	**5·22**	5·25	**3·26**	3·35
120-min prediction	**5·33**	5·38	**3·36**	3·48
180min prediction	**5·41**	5·42	**3·41**	3·47

DOI: 10.1002/hyp

Table VIII. Mean correlation coefficient (MCC) and mean critical success index (MCSI) values comparison (August 1992 event)

Lead-time	MCC		MCSI (%)	
	Deterministic	Stochastic	Deterministic	Stochastic
60-min prediction	0·164	**0·252**	**50·5**	49·1
120-min prediction	0·063	**0·173**	42·1	**46·6**
180-min prediction.	0·052	**0·143**	36·6	**45·7**

Table IX. Mean correlation coefficient (MCC) and mean critical success index (MCSI) values comparison (June 1993 event)

Lead-time	MCC		MCSI (%)	
	Deterministic	Stochastic	Deterministic	Stochastic
60-min prediction	0·216	**0·229**	**74·03**	69·45
120-min prediction	0·090	**0·123**	65·15	**66·73**
180-min prediction	0·070	**0·072**	56·51	**64·86**

the 50 sets of stochastic prediction results. From both the tables, the values represent that stochastic prediction gives improved accuracy compared to the deterministic predictions while the accuracy decreases as prediction lead-time gets longer.

ENSEMBLE RUNOFF SIMULATION WITH A DISTRIBUTED HYDROLOGIC MODEL

Model introduction

For real-time flood forecasting, there has been considerable interest in utilizing weather radar and distributed hydrologic models, as it can provide continuous spatiotemporal measurements and outputs that are immediately available at any location in a catchment. From a hydrological point of view, runoff responses of forecasted rainfall throughout a hydrologic system are valuable information for checking the validity of the input data during operational usage. This study assesses the validity of stochastic prediction fields using a distributed hydrologic model, which is developed for the Yodo-River basin located in the Miyama radar observation range.

The Yodo-River model (Sayama *et al*., 2006) used here solves kinematic wave equations for both subsurface flow and surface flow using the Lax-Wendroff scheme. Discharge and water depth diffuse node to node according to a predefined routine order, which is determined in accordance with Digital Elevation Model (DEM) and river channel network data. The eight-direction flow map is prepared for defining the routing order for water flow diffusion as shown in Figure 10. One characteristic of the Yodo-River model is a specific stage-discharge relationship, which incorporates saturated and unsaturated flow mechanisms as Equation (18):

$$q(h) = \begin{cases} v_c d_c (h/d_c)^{\beta}, (0 \le h < d_c) \\ v_c d_c + v_a (h - d_c), (d_c \le h < d_s) \\ v_c d_c + v_a (h - d_c) + \alpha (h - d_s)^m, (d_s \le h) \end{cases} \quad (18)$$

In the equation, when water depth h is less than the depth of the capillary pore layer d_c $(0 \le h < d_c)$, flow

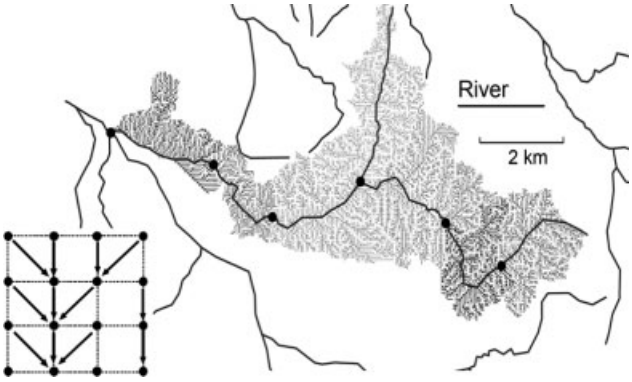

Figure 10. Flow direction map included in the Yodo-River model. Using the Kinematic wave equation, discharges and water depths diffuse node to node according to a predefined routing order, which is determined in accordance with DEM and river channel network data

is described by Darcy's law with a degree of saturation $(h/d_c)^{\beta}$ and a saturated velocity $v_c (= k_c \times i)$. Here, β is the degree of saturation ratio, k_c is saturated hydraulic conductivity in the capillary layer, and i is the slope gradient. If h increases $(d_c \le h < d_s)$, the velocity of flow from the non-capillary pore layer is expressed as v_a $(= k_a \times i)$, where k_a is the saturated hydraulic conductivity in the non-capillary layer. When the water depth is greater than that of the soil layer $(d_s \le h)$, overland flow is added using Manning's resistance law using $\alpha = i^{1/2}/n$, $m = 5/3$ and the roughness coefficient n.

Model parameters in the stage–discharge relationship are d_c, d_s, k_c, k_s and n, and β $(= v_a/v_c)$ is determined by the continuity condition on the wave celerity. This specific stage-discharge relationship characterizes the model and as a result, each cell has its own stage-discharge relationship determined by topography, land use, and soil type (Tachikawa *et al*., 2004). Details on the Yodo-River model are given by Sayama *et al*. (2006).

Simulation methodology

The runoff simulation is carried out in three different catchments located within the observation range of the Miyama radar: Ootori (156 km^2), Ieno (476 km^2)

DOI: 10.1002/hyp

and Kamo (1469 km^2) (Figure 1). The parameters were calibrated prior to performing the ensemble runoff simulation, using the Miyama radar observation and observed discharge data for each outlet. The purpose of this runoff simulation is to examine the accuracy and reliability range of the stochastic rainfall prediction from a hydrological point of view. Thus, the discharge simulated using the deterministic prediction and the ensemble discharge using the stochastic prediction is compared.

For each lead-time prediction from both events, the 50 sets of stochastic prediction fields generate an ensemble runoff simulation through the distributed hydrologic model. Each stochastic prediction field among the 50 sets of input data was assigned to each runoff simulation independently. Firstly, preliminary simulation was conducted with the observed rainfall data until 00 : 00 h on August 18 for the August 1992 event and until 06 : 00 h on June 30 for the June 1993 event. The deterministic and stochastic prediction data were inputted after the abovementioned times. The ensemble simulation was carried out until 00 : 00 h on August 20 (August 1992 event) and until 18 : 00 h on June 30 (June 1993 event). After those periods, the observed rainfall data were equally set to every 50-ensemble simulations, and the simulation was shortly continued in order to observe the remaining effect of the input rainfall on the runoff. The rainfall data, whether observed or predicted, were given every 5 min for the distributed hydrologic model, which produced a hydrograph every 10 min.

Runoff simulation results and discussion

Figure 11 shows the ensemble runoff simulation results (60-min prediction) in the August 1992 event and the June 1993 event respectively, for all three subject basins: Ootori (156 km^2), Ieno (476 km^2) and Kamo (1469 km^2). The black thick line stands for the discharge from the observed radar rainfall, which is the reference discharge regarded as the actual value. The thick grey line represents the discharge from the original deterministically predicted rainfall, and the 50 thin grey lines show each discharge from the stochastic prediction fields.

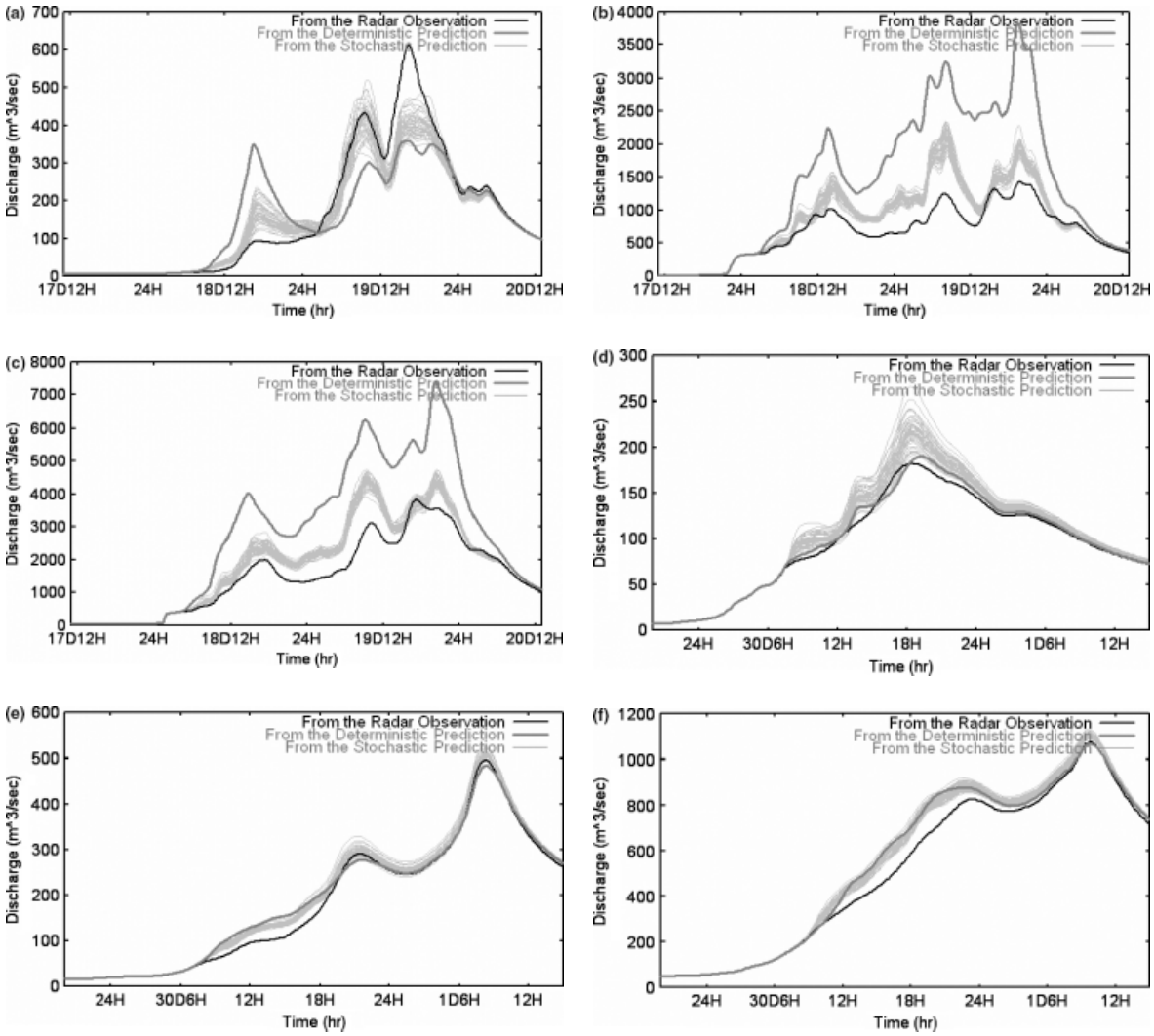

Figure 11. Discharge hydrograph from the radar observation, deterministic, and stochastic prediction [using 60-min prediction rainfall data of August 1992 event (left) and June 1993 event (right)]. Fifty hydrographs from the stochastic rainfall data produce an improved ensemble simulation of discharges

DOI: 10.1002/hyp

In the results of the August 1992 event (Figure 11a, b and c), the discharges from the stochastic rainfall data show closer values to the reference discharges, suggesting that the prediction accuracy of the stochastic prediction has improved. The ensemble simulation using the stochastic rainfall prediction clearly shows the improved prediction accuracy with the reduced discharge compared to the output from the deterministic rainfall data. While the forecast accuracy improvement is encouraging, it is hard to determine whether the band, which stands for the reliability range of the stochastic prediction, is acceptable. In the case of the June 1993 event (Figure 11d, e and f), the ensemble runoff simulation results do not show clear improvement compared to the discharges from the deterministic prediction. As discussed in the forecast verification section, the June 1993 event has low rainfall intensities and the accuracy improvement through the error simulation may not work properly for this event.

Note that the runoff simulation results were given by the continuous application of the stochastic prediction data; therefore, the discharge output accumulated the prediction error. In practical application of real-time rainfall forecasting, the rainfall input data will be given in accordance with the most updated forecast for each lead-time; therefore the accumulated prediction error will not be included in the discharge output.

For an overall comparison of the runoff simulation, peak discharges of each case from both events are extensively examined, and those values are presented in Tables X and XI. In the case of the August 1992 event, the peak discharges form the deterministic prediction give variant values showing large overestimation in most cases. However, the stochastic prediction using the error simulation model decreases the overestimation of discharge in most cases. The closer values that stand for accuracy improved results are marked using bold characters in those tables.

In the results from the June 1993 event (Table XI), about half of the runoff simulation results using the stochastic rainfall data do not produce positive results with a reasonable reliability range. For Ieno and Kamo basins, the deterministic prediction already provides highly accurate peak discharge values, and the ensemble forecasting using the stochastic rainfall data fails to offer much more accurate and reasonable reliability. This result may be because of a certain characteristic in the June 1993 event as mentioned in the earlier section including low rainfall intensities.

The ACRA values are calculated using the rainfall data on each testing basin, and the values are presented in Tables XII and XIII. The ACRA values of each basin have similar patterns to the earlier analysis using the overall rainfall amount within the radar range; the values from the stochastic rainfall data provide not only improved results but also an improved reliability range. The ACRA in the August 1992 event is rather large when

Table X. Peak discharge comparison of August 1992 event (Unit: m^3/s)

Basin	Prediction lead-time	Observation	Deterministic prediction	Stochastic prediction	
				Mean	Min∼Max
Ootori (156 km^2)	60 min	610·3	358·9	**432·1**	378·0 ∼ 520·3
	120 min	610·3	913·4	**622·5**	542·7 ∼ 694·3
	180 min	610·3	1096·2	**866·9**	664·1 ∼ 1040·3
Ieno (476 km^2)	60 min	1426·7	3838·6	**2108·4**	1882·5 ∼ 2348·5
	120 min	1426·7	2534·7	**1947·4**	1728·6 ∼ 2175·2
	180 min	1426·7	454·3	**1259·9**	1095·5 ∼ 1463·2
Kamo (1469 km^2)	60 min	3836·1	7362·8	**4474·8**	4063·2 ∼ 4743·4
	120 min	3836·1	7271·0	**5385·6**	4939·0 ∼ 6034·5
	180 min	3836·1	**4470·3**	4718·8	4343·5 ∼ 5271·2

Table XI. Peak discharge comparison of June 1993 event (Unit: m^3/s)

Basin	Prediction lead-time	Observation	Deterministic prediction	Stochastic prediction	
				Mean	Min∼Max
Ootori (156 km^2)	60 min	181·8	**190·2**	218·6	191·5 ∼ 265·3
	120 min	181·8	120·7	**201·2**	179·0 ∼ 228·1
	180 min	181·8	111·3	**188·9**	161·6 ∼ 213·1
Ieno (476 km^2)	60 min	496·2	484·3	**504·6**	487·4 ∼ 527·3
	120 min	496·2	**479·2**	552·2	538·5 ∼ 569·4
	180 min	496·2	430·3	**501·5**	481·5 ∼ 522·9
Kamo (1469 km^2)	60 min	1073·6	**1067·2**	1104·5	1087·2 ∼ 1131·2
	120 min	1073·6	**1043·8**	1190·5	1162·9 ∼ 1218·6
	180 min	1073·6	918·0	**1083·2**	1052·9 ∼ 1112·5

DOI: 10.1002/hyp

Table XII. Accumulated rainfall amount (ACRA) values on each basin (August 1992 event, Unit: *mm/h*)

Basin	Prediction lead-time	Observation	Deterministic prediction	Stochastic prediction	
				Mean±StDev	Min∼Max
Ootori (156 km^2)	60 min	273·2	341·6	**331·3** ± 24·2	284·7 ∼ 376·8
	120 min	273·2	442·8	**357·9** ± 27·0	281·0 ∼ 416·5
	180 min	273·2	593·8	**459·3** ± 30·9	390·7 ∼ 507·0
Ieno (476 km^2)	60 min	362·7	818·9	**487·5** ± 27·2	424·4 ∼ 537·7
	120 min	362·7	437·3	**413·4** ± 26·4	350·4 ∼ 477·4
	180 min	362·7	80·0	**300·3** ± 18·9	258·4 ∼ 352·1
Kamo (1469 km^2)	60 min	319·6	574·4	**389·2** ± 14·7	357·8 ∼ 418·4
	120 min	319·6	533·5	**387·4** ± 18·9	340·5 ∼ 421·1
	180 min	319·6	238·9	**312·4** ± 13·3	258·9 ∼ 336·4

Table XIII. Accumulated rainfall amount (ACRA) values on each basin (June 1993 event, Unit: *mm/h*)

Basin	Prediction lead-time	Observation	Deterministic prediction	Stochastic prediction	
				Mean±StDev	Min∼Max
Ootori (156 km^2)	60 min	58·2	55·2	**60·5** ± 7·1	46·1 ∼ 80·2
	120 min	58·2	27·6	**51·1** ± 6·0	39·9 ∼ 66·0
	180 min	58·2	39·7	**63·2** ± 7·9	48·5 ∼ 88·1
Ieno (476 km^2)	60 min	41·5	**50·0**	53·8 ± 3·1	47·5 ∼ 60·2
	120 min	41·5	**53·0**	62·1 ± 3·5	54·0 ∼ 71·6
	180 min	41·5	**44·4**	59·0 ± 4·5	45·4 ∼ 68·0
Kamo (1469 km^2)	60 min	41·7	**51·4**	54·2 ± 2·3	50·3 ∼ 60·6
	120 min	41·7	**47·1**	58·7 ± 2·9	49·9 ∼ 63·5
	180 min	41·7	**36·8**	54·7 ± 3·5	47·8 ∼ 62·1

considering that it is within two days' accumulation, while the amount in the June 1993 event is small. The proposed algorithm for the stochastic forecasting of precipitation has some possibility to work more properly when there is a severe rainfall event, which is more practical for the purpose of flood forecasting.

CONCLUSIONS

For forecast accuracy improvement and ensemble flood forecasting with an external error consideration, this study introduced ensemble rainfall forecasting using a stochastic error field simulation along with a runoff simulation using a distributed hydrologic model. The proposed algorithm is for offering probable variation of the deterministic prediction results from the extrapolation model, as well as for improving its forecast accuracy.

The translation model predicted the radar rainfall field, and the prediction error structure was thus spatially and temporally analysed. The random error fields were simulated using the error structure, the stochastic prediction field, which is the combination of the deterministic rainfall and the simulated error, was generated, and its stochastic validity was examined. The stochastic prediction fields not only gave probable reliability with variant form of rainfall fields but also improved the accuracy of the deterministic prediction.

The validation of the stochastic prediction fields was completed from two different perspectives: checking the performance of the rainfall prediction using various indexes, and comparing hydrographs simulated through a distributed hydrologic model. Firstly, for an overall forecast verification, several performance indices, such as ACRA, RMSE and MAE were adopted. From the ACRA testing, the reliability ranges of the ensemble forecasting using stochastic rainfall data clearly expressed the uncertainty of the forecasted values; the greater the prediction lead-time is extended, the wider the range becomes. RMSE and MAE indices also demonstrate accuracy improvement from the stochastic prediction.

Secondly, the ensemble runoff simulation with the Yodo-River model verified the hydrologic effectiveness of the stochastic prediction fields. While the ensemble runoff simulation using the stochastic rainfall data showed highly encouraging results, the reliability range of the stochastic prediction needs to be more carefully verified on the basis of various event types in order to confirm the proposed ensemble forecasting method.

REFERENCES

Bellon A, Austin GL. 1984. The accuracy of short-term radar rainfall forecasts. *Journal of Hydrology* **70**: 35–49.

Collier CG, Krzysztofowicz R. 2000. Preface: Quantitative precipitation forecasting. *Journal of Hydrology* **239**: 1–2.

Davis MW. 1987. Generating large stochastic simulation-The matrix polynomial approximation method. *Mathematical Geology* **19**(2): 99–107.

Du J, Mullen SL. 1997. Short-range ensemble forecasting of quantitative precipitation. *Monthly Weather Review* **125**: 2427–2459.

Fox NI, Wilson JW. 2005. Very short period quantative precipitation forecasting. *Atmospheric Science Letters Wiley Interscience* **6**: 7–11.

Ganguly AR, Bras RL. 2003. Distributed quantitative precipitation forecasting using information from radar and numerical weather prediction models. *Journal of Hydrometeorology American Meteorological Society* **4**: 1168–1180.

Georgakakos KP. 2000. Covariance propagation and updating in the context of real-time radar data assimilation by quantitative precipitation forecast models. *Journal of Hydrology* **239**: 115–129.

Georgakakos KP, Bras RL. 1984. A hydrologically useful station precipitation model: 1.Formulation. *Water Resources Research* **20**(11): 1585–1596.

Golding BW. 2000. Quantitative precipitation forecasting in the UK. *Journal of Hydrology* **239**: 286–305.

Grecu M, Krajewski WF. 2000. A large-sample investigation of statistical procedures for radar-based short-term quantitative precipitation forecasting. *Journal of Hydrology* **239**: 69–84.

Kawamura A, Jinno K, Berndtsson R, Furukawa T. 1997. Real-time tracking of convective rainfall properties using a two-dimensional advection-diffusion model. *Journal of Hydrology* **203**: 109–118.

Krzysztofowicz R. 2001. The case for probabilistic forecasting in hydrology. *Journal of Hydrology* **249**: 2–9.

Leith CE. 1974. Theoretical skill of Monte Carlo forecasts. *Monthly Weather Review* **102**: 409–418.

Lovejoy S, Schertzer D. 1986. Scale invariance, symmetries fractals and stochastic simulations of the atmosphere. *Bulletin of the American Meteorological Society* **67**: 21–32.

Marshall JS, Palmer WM. 1948. The distribution of raindrops with size. *Journal of Meteorology* **5**: 165–166.

Nakakita E, Ikebuchi S, Nakamura T, Kanmuri M, Okuda M, Yamaji A, Takasao T. 1996. Short-term rainfall prediction method using a volume scanning radar and grid point value data from numerical weather prediction. *Journal of Geophysical Research* **101**(D21): 26181–26197.

Nakakita E, Ikebuchi S, Shiiba M, Takasao T. 1990. Advanced use into rainfall prediction of three-dimensionally scanning radar. *Stochastic Hydrology and Hydraulics* **4**: 135–150.

Sayama T, Tachikawa Y, Takara K, Ichikawa Y. 2006. Distributed Rainfall-Runoff Analysis in a Flow Regulated Basin Having Multiple Multi-Purpose Dams. In *Predictions in Ungauged Basins:Promises and Progress*, IAHS Publication No. 303, International Association of Hydrological Sciences: Wellingford, UK, 371–381.

Shiiba M, Takasao T, Nakakita E. 1984. Investigation of short-term rainfall prediction method by a translation model. *Annual Journal of Hydraulic Engineering, JSCE* **28**: 423–428, (Japanese).

Smith KT, Austin GL. 2000. Nowcasting precipitation-a proposal for a way forward. *Journal of Hydrology* **239**: 34–45.

Tachikawa Y, Komatsu Y, Takara K, Shiiba M. 2003. Stochastic modeling of the error structure of real-time predicted rainfall and rainfall field generation. In *Weather Radar Information and Distributed Hydrological Modelling*, IAHS Publication No. 282, International Association of Hydrological Sciences: Wellingford, UK, 66–74.

Tachikawa Y, Nagatani G, Takara K. 2004. Development of stage-discharge relationship equation incorporating saturated-unsaturated flow mechanism. *Annual Journal of Hydraulic Engineering, JSCE* **48**: 7–12, (Japanese with English abstract).

Tachikawa Y, Shiiba M. 2000. Gaussaian and log-normal random field generation based on the square root decomposition of a covariance matrix. *Journal of Hydraulic, Coastal and Environmental Engineering, JSCE* **656**(II-52): 39–46.

Takasao T, Shiiba M, Nakakita H. 1994. A real-time estimation of the accuracy of short-term rainfall prediction using radar. *Stochastic and Statistical Methods in Hydrology and Environmental Engineering* **2**: 339–351.

Wilson JW, Crook NA, Mueller CK, Sun J, Dixon M. 1998. Nowcasting thunderstorms: A status report. *Bulletin of the American Meteorological Society* **79**(10): 2079–2099.

DOI: 10.1002/hyp